Annual Cycle of Subsurface Thermal Structure in the Tropical Atlantic Ocean

STEFAN HASTENRATH

Department of Meteorology, University of Wisconsin, Madison

JACQUES MERLE

ORSTOM/LPDA, University of Paris VI

ABSTRACT

The subsurface thermal structure in the tropical Atlantic Ocean (30°N–20°S, East of 80°W) is studied on the basis of an extensive data bank of subsurface soundings. Calendar monthly maps are presented showing mixed layer depth, base of thermocline, thermocline thickness, and vertical temperature gradient across the thermocline. These maps are complemented by vertical cross sections depicting mixed layer depth, base of thermocline, and selected isotherms: a zonal profile along the equator (50°W–10°E), a meridional transect across the Eastern Atlantic (4°N–18°S), and a meridional section across the Central Atlantic (30°N–18°S).

The basinwide subsurface thermal structure is dominated by the annual cycle of the surface wind field with extrema around April and August. The mixed layer is relatively shallow between 20°N and 10°S, with overall greater depth in the western as compared to the eastern portion of the basin. Two systems of annual cycle variation of mixed layer depth stand out. (i) Along the equator, the mixed layer depth increases from around April to about August, with largest variations to the west, in direct response to the annual variation of the zonal wind component in the equatorial zone. (ii) In the North Equatorial Atlantic, a northward migration of a band of shallowest mixed layer is apparent from April to August, broadly concordant with the seasonal migration of the confluence zone between the northeast trades and the cross-equatorial airstreams from the Southern Hemisphere. Concomitant with this northward displacement, a belt of maximum mixed layer depth builds up immediately to the north of the equator. The evolution of this trough–ridge structure in mixed layer depth is related to the seasonal reversal of the North Equatorial Countercurrent. Various recent numerical model experiments are in qualitative agreement with the present empirical documentation of the annual cycle of the basinwide pattern of mixed layer depth.

The thermocline is likewise thinnest and most intense in the low latitudes, especially in the eastern portion of the basin, but its spatial pattern and seasonal variations differ from those of the mixed layer. The near-equatorial thermocline structure is characterized by a wide vertical separation of isothermal surfaces at the Equator and extremum zones of thinnest and most intense thermocline at 4°S year round and at 4°N especially in the latter part of the boreal winter semester. It is conjectured that easterly surface winds produce, at the equator, upwelling above and downwelling below the thermocline and the opposite pattern of vertical motion at some distance from the equator, thus leading to the observed thick and weak thermocline at the equator and the isotherm packing around 4°N and S. The marked asymmetry of the surface wind field and the associated wind stress curl pattern within the cross-equatorial airstreams at the height of the boreal summer may be factors for the absence of this extremum zone of thermocline characteristics at 4°N at this time of the year. The comprehensive documentation of subsurface thermal structure presented here is relevant in recent and ongoing empirical and modeling studies of the tropical Atlantic Ocean.

1. Introduction

The role of the tropical oceans in the functioning of the global climate system is increasingly being recognized in national and international planning documents (World Meteorological Organization, 1980, pp. 12–13, 39–41; National Climate Program Office, 1980, p. 46–50; National Academy of Sciences, 1983, p. 10–21; World Meteorological Organization—ICSU, 1983, vol. 1, p. 1–20; Anonymous, 1984), of key importance being the coupling between the lower atmosphere and the upper hydrosphere. In the Atlantic, a background climatology of the surface atmospheric circulation and

oceanic heat budget has been produced nearly a decade ago (Hastenrath and Lamb, 1977, 1978), and this has served as a basis for investigations into the mechanisms of interannual climate variability of various circum-Atlantic regions (review in Hastenrath, 1984).

The time appears ripe to complement these studies of the lower atmosphere by a background climatology of the upper ocean. Important steps in this direction have recently been made by the SEQUAL and FOCAL programs (Anonymous, 1981; Merle, 1980c). An updated bank of subsurface soundings compiled by the French Navy provided the data source for a series of recent empirical analyses (Merle, 1983; Merle and Ar-

nault, 1985; Hastenrath and Merle, 1986), which substantially expand on previous work (Robinson et al., 1979; Levitus, 1982, 1984; Lamb, 1984). The present paper offers, for the first time, a comprehensive documentation of the subsurface thermal structure of the tropical Atlantic Ocean in the course of the year. Such an evaluation of the observed structure of the upper ocean and its annual cycle is expected to serve as an essential reference for the growing field of numerical modeling studies, and to provide a background for empirical investigations into the annual cycle functioning of the combined atmosphere–ocean system in the Atlantic domain.

2. Observations and basic data processing

The following description of the subsurface data bank is in part repeated from Hastenrath and Merle (1986). Subsurface temperature soundings in the tropical Atlantic between 30°N and 20°S and East of 80°W were compiled by the French Navy (Merle, 1983; Merle and Arnault, 1985). The data bank comprises 51 782 expendable bathythermograph (XBT), 93 525 mechanical bathythermograph (MBT) soundings, and 28 557 hydrocasts (station data), a total of 173 864 soundings. Most profiles stem from the U.S. National Oceanographic Data Center (NODC), but also included are additional XBT from the French Navy, Nansen CTD casts from the oceanographic vessel *Capricorne*, as well as soundings from various early expeditions, namely the *Meteor* in 1924, the *Atlantis* in 1931, the *Discovery* in 1935, the *Crawford* in 1957, and the *Equalant* in 1962–63, and GATE data. In general, the collections terminate in 1978. The distribution of observations is irregular in space and time.

Data were processed by two degree latitude and four degree longitude areas as shown in Fig. 1. For each block, each calendar month, and each type of data (XBT, MBT, Nansen), soundings were evaluated in context. Profiles, which at any standard level showed temperature values departing by more than two standard deviations from the mean of all profiles, were rejected at all levels. For the area average profile, the three types of data were weighted according to the number of soundings retained. It is estimated that as a result the uncertainty of temperature values at each standard level is reduced to less than 0.1°C. However, for the regions of better coverage such as the Gulf of Guinea and the equatorial zone as a whole, and the layers outside the thermocline, the data are considered to be better than 0.05°C. Information was thus compiled for the standard depth 0, 5, 10, 20, 30, 40, 50, 60, 75, 100, 125, 150, 200, 250, 300, 400, 500 m, etc. The spatial distribution of soundings is also illustrated in Fig. 1. The density of observations broadly decreases southward and with depth. Hastenrath and Merle (1986, Table 1) describe the variation of observations with depth, and compare the data volume of the present
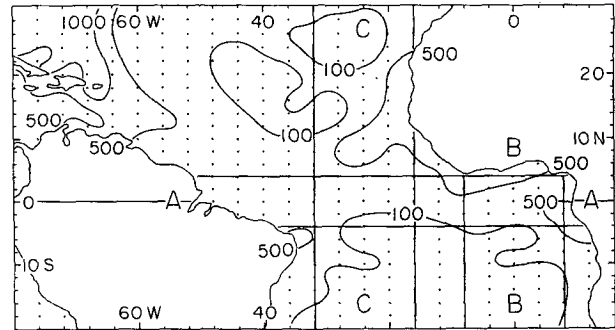

FIG. 1. Orientation map showing breakdown into rectangles of 2° latitude by 4° longitude, number of soundings per rectangle, and location of zonal (A) and meridional (B and C) cross sections in Figs. 6–8.

study with the publications of Robinson et al. (1979), Lamb and Bunker (1982), and Levitus (1982, 1984). The present data compilation is considerably more plentiful than those of Levitus (1982, 1984), Lamb and Bunker (1982), and of Robinson et al. (1979) which moreover terminates at 150 m.

In the analysis of subsurface observations the following criteria were used. The depth at which temperature is 1°C lower than at the surface is chosen as mixed layer depth (Figs. 2, 6–8), or top of the thermocline. The base of the thermocline (Figs. 3, 6–8) is defined as the level from which downward the temperature decreases by less than 2°C over a 50 m interval. Thermocline thickness (Fig. 4) is the vertical distance between thermocline base and top. The temperature gradient across the thermocline (Fig. 5) is the ratio of temperature difference between top and base of the thermocline over thermocline thickness.

3. Analysis and presentation

The central objective of this study is to ascertain the annual cycle and spatial patterns of upper-ocean temperature structure in the tropical Atlantic, so as to produce the documentation needed for numerical model simulations, as well as for empirical investigations of atmosphere–hydrosphere coupling on the climatic time scale. To this end, calendar monthly maps are produced, in the first place, of pertinent parameters of the oceanic thermal structure. The parameters chosen here are defined in section 2.

Of foremost interest is the depth of the mixed layer (Fig. 2), representing the portion of the hydrospheric column in which the influences of surface heat exchange and surface wind stress forcing are concentrated. It is therefore not surprising that this parameter has been chosen for presentation in various earlier studies of subsurface temperature conditions (Wyrtki, 1971; Robinson et al., 1979; Lamb, 1984). Inasmuch as the thickness of the thermocline exhibits conspicuous
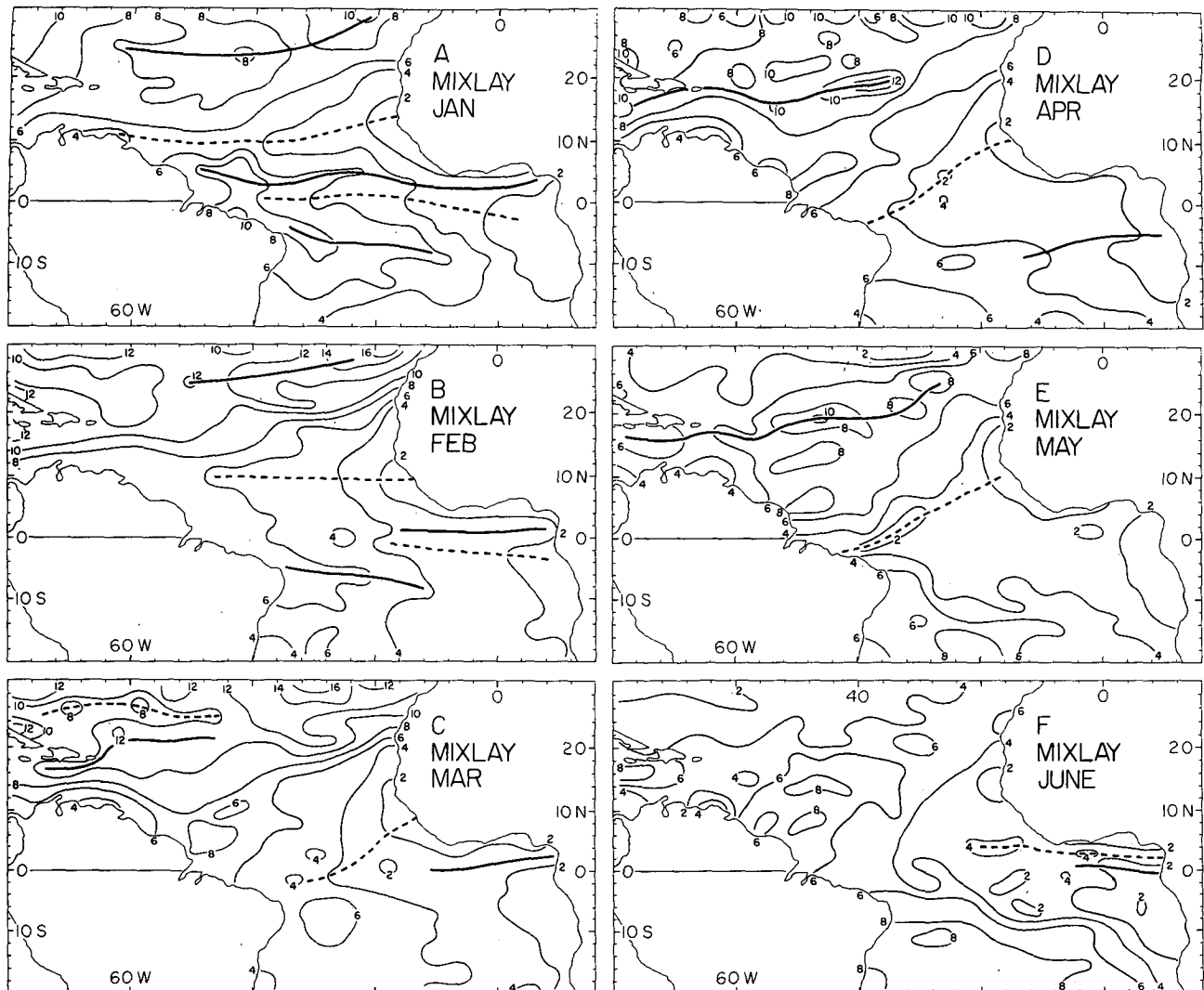
FIG. 2. Monthly maps of mixed layer depth in tens of meters. Heavy solid lines denote relative maxima, and heavy broken lines relative minima. Parts A–F: January, February, March, April, May, June.

variations both spatially and in the course of the year, which appear at least in part related to the surface wind stress forcing, it was found appropriate to map, in addition to the mixed layer depth (Fig. 2; section 3a), also the thermocline base (Fig. 3; section 3b), and thermocline thickness (Fig. 4; section 3c). The latter two parameters are not commonly found in subsurface temperature evaluations. The topography of certain isothermal surfaces (Merle, 1983) bears some resemblance to the distribution of thermocline base. The three aforementioned parameters, mixed layer depth, thermocline base, and thermocline thickness, while exhibiting coherent patterns, offer no clue on the remarkable spatial and temporal differentiations in thermocline intensity. In order to capture this important feature of subsurface thermal structure, the temperature gradient across the thermocline (Fig. 5; section 3d) was also mapped here.

The mapping of the four indicative parameters discussed above is complemented by vertical cross sections at three strategic locations, as shown in Fig. 1. The marked seasonal changes of thermal structure in the equatorial–vertical plane (Fig. 6; section 3e) have been discussed in previous studies (Merle, 1980a,b, 1983; Hastenrath and Merle, 1986). The meridional–vertical cross section in the eastern Atlantic (Fig. 8, section 3f) traverses the tongue of cold surface waters immediately to the south of the equator, which becomes particularly prominent at the height of the boreal summer. The meridional–vertical transect across the central Atlantic (Fig. 10, section 3g) encompasses, among other features, the domain of the "amphibious intertropical convergence zone complex" in the low-latitude North Atlantic (Hastenrath and Lamb, 1977, charts 14–25, 50–61), and thus documents seasonal developments in subsurface thermal structure pertinent to a particularly
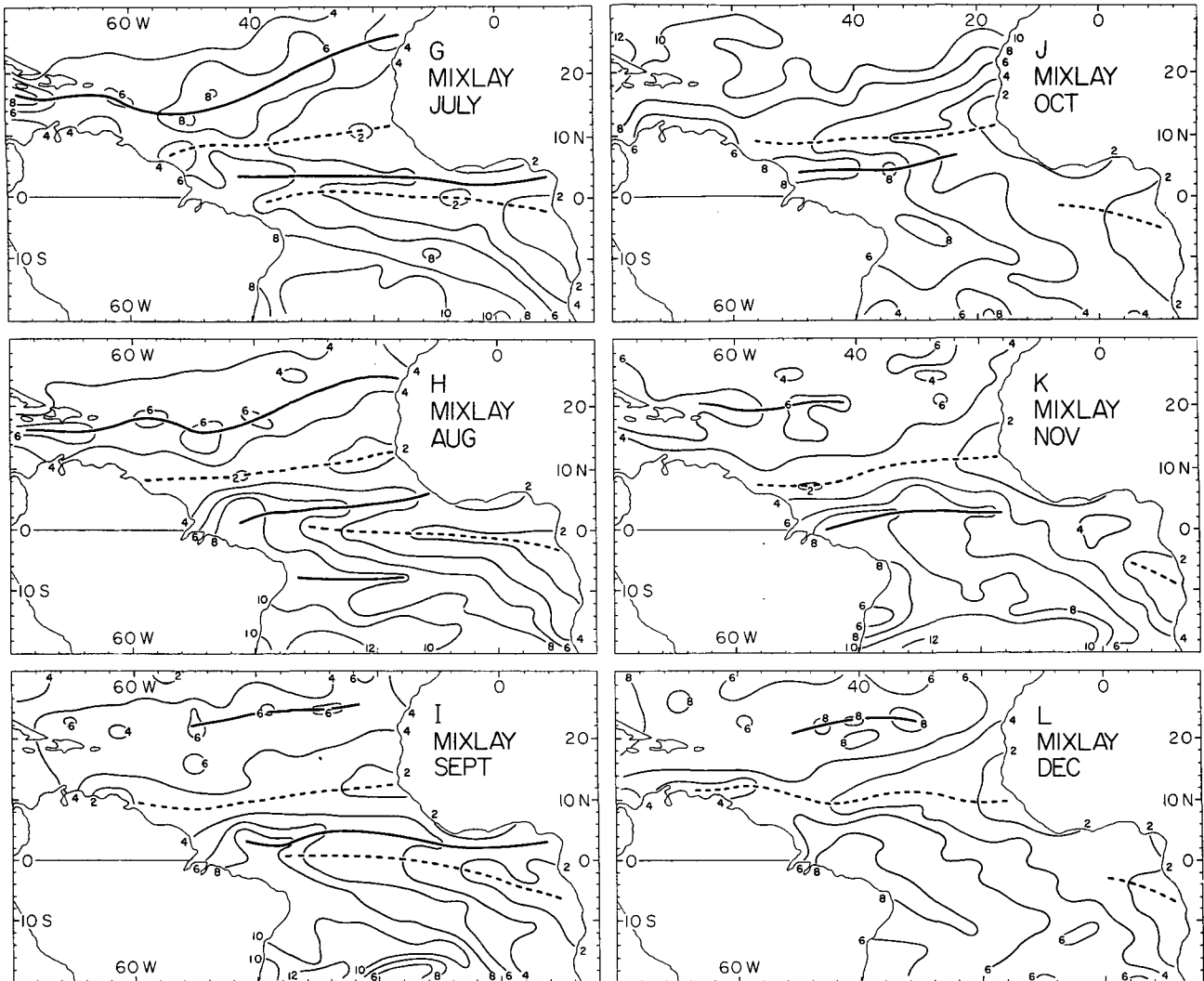
FIG. 2. (*Continued*). Parts G–L: July, August, September, October, November, December.

prominent quasi-permanent circulation system of the lower atmosphere. All of these cross sections are constructed from observations averaged over broad bands (ref. Fig. 1), thus ensuring considerable data stability. The topographies of thermocline top and base entered in the cross sections Figs. 6, 8, and 10, in addition to the isotherms are intended to facilitate the comparison with the maps, Figs. 2–4.

a. Mixed layer depth

Calendar monthly maps of mixed layer depth are presented in Fig. 2. Throughout the year and for the basin as a whole, the mixed layer tends to be deeper in the western as compared to the eastern portion of the tropical Atlantic. During the boreal winter semester (November–April), the mixed layer is particularly deep in the northern portion of the map area, while a zone of smallest values is found broadly between the equator

and 20°N, extending from the coast of northern South America to West Africa. From around April to August, this band of shallowest mixed layer becomes more distinct and migrates northward. Concurrently, the mixed layer in the northern portion of the map area shallows. At the height of the boreal summer, a tongue of shallow mixed layer immediately to the south of the equator extends from the African coast to the central portion of the ocean, broadly concordant with the well-documented tongue of cold surface waters (Hastenrath and Lamb, 1977, charts 56–57). At the same time, the mixed layer deepens in a tongue just to the north of the equator, most notably in the western portion of the basin. After August, the mixed layer deepens in the northern portion of the map area, the band of shallow thermocline stretching from the Caribbean to West Africa shifts southward, the tongue of shallow mixed layer immediately to the south of the equator disap-
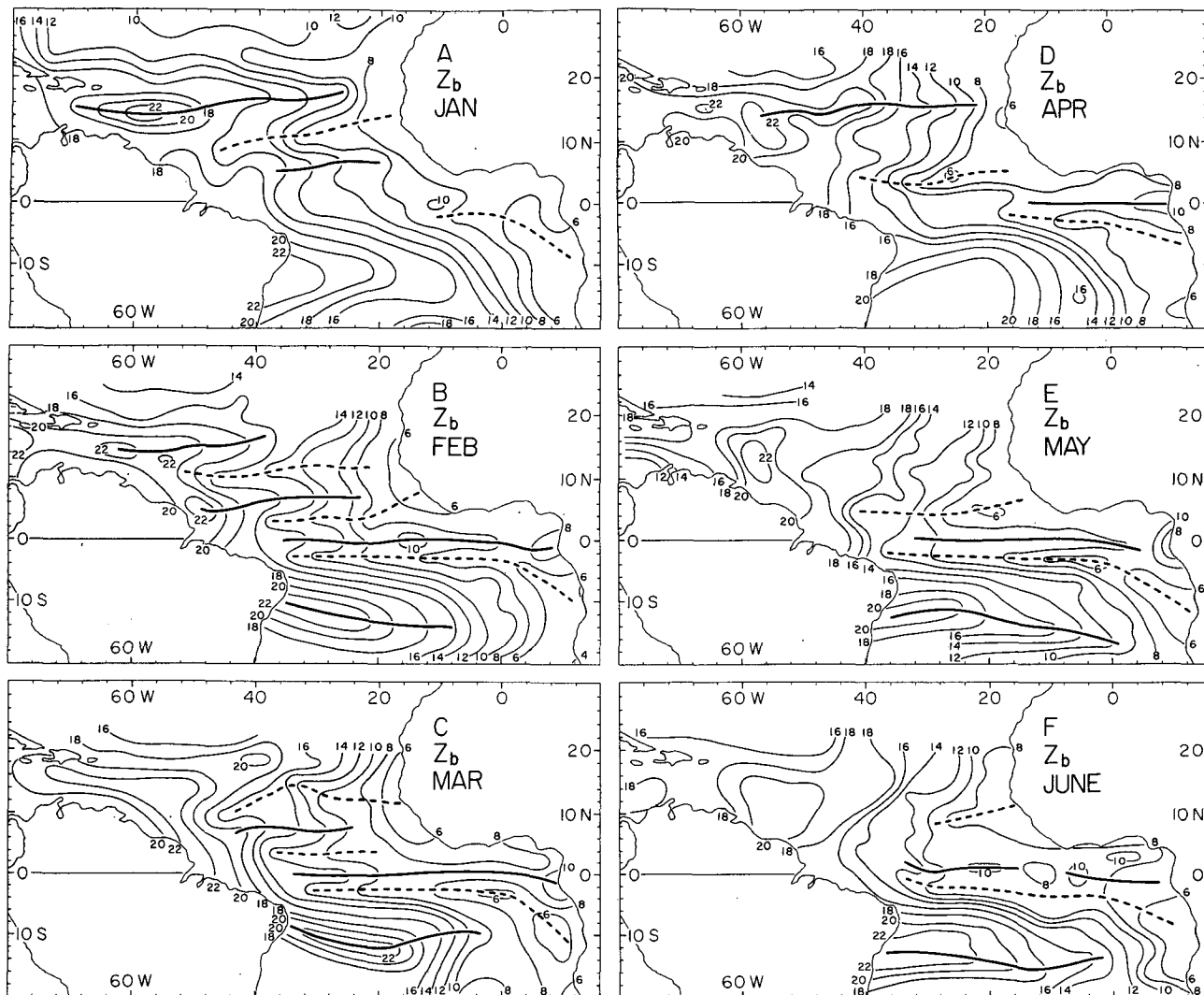
FIG. 3. Monthly maps of base of thermocline, in tens of meters. Heavy solid lines denote relative maxima,
and heavy broken lines relative minima. Parts A–F: January, February, March, April, May, June.

pears, so that the enclosed zone of relative maximum is eliminated, and the mixed layer in the southernmost portion of the map area becomes shallower.

The patterns of mixed layer depth resemble the annual cycle of the field of surface dynamic topography (Merle and Arnault, 1985, Fig. 8), which in July and August also shows a succession of approximately zonally oriented troughs and ridges, and an intensification of a trough to the south and of a ridge to the north of the equator. The latter feature is directly related to enhancement of the North Equatorial Countercurrent at the height of boreal summer (Garzoli and Katz, 1983; du Penhoat and Tréguier, 1984; Philander and Pacanowski, 1984).

Prominent pattern changes documented in the map sequence of Fig. 2 appear related to the annual cycle of the surface wind field and to the sea surface temperature pattern (Hastenrath and Lamb, 1977, charts 14–25, 50–61). Thus, the northward migration of the zone of shallowest mixed layer, extending from the coast of northern South America to West Africa, from around April to August, parallels the northward shift of a quasi-permanent discontinuity in the surface wind field and associated maximum of wind stress curl and Ekman pumping, as well as the northward displacement of the band of warmest surface waters. Likewise, the tongue of shallowest mixed layer immediately to the south of the equator in the eastern Atlantic in July and August coincides in timing with the most conspicuous development of the tongue of cold surface waters. Possible contributing mechanisms include remote wind stress forcing in the western portion of the basin generating eastward propagating Kelvin waves (Moore et al., 1978; Servain et al., 1982; Busalacchi
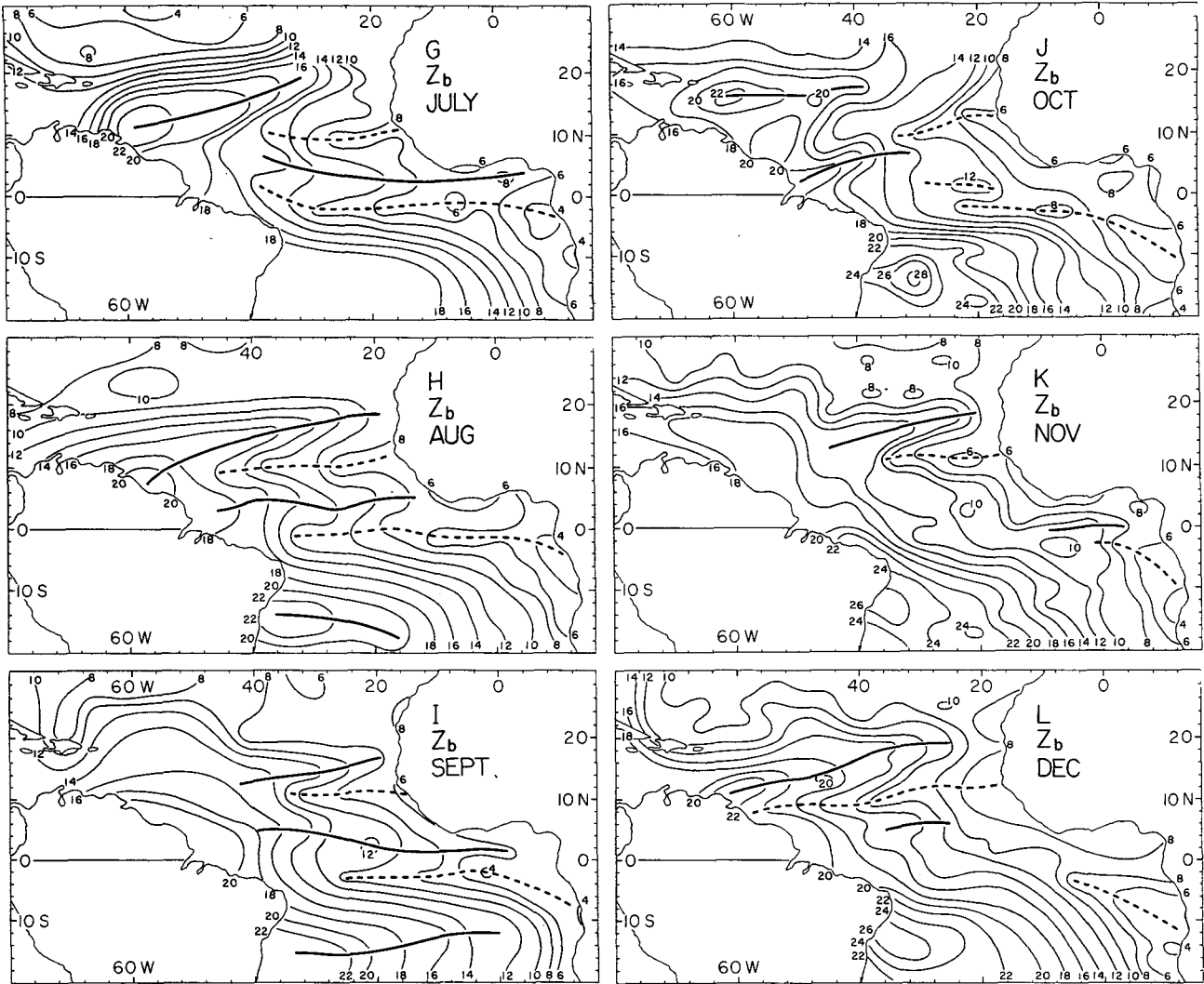
FIG. 3. (Continued). Parts G–L: July, August, September, October, November, December.

and Picaut, 1983; Houghton, 1983; Weisberg and Tang, 1983; Cane and Patton, 1984) and in-situ wind stress forcing in the eastern Atlantic associated with the intensification of the cross-equatorial airflow during boreal summer (Philander, 1978). It is noteworthy that both mixed layer depth (Fig. 2) and sea surface temperature (Hastenrath and Lamb, 1977, charts 50–61) show a marked hemispheric asymmetry concordant with that of the surface wind field (Hastenrath and Lamb, 1977, charts 14–25), and that these asymmetries in the uppermost ocean layer are most pronounced during the boreal summer half-year, when the asymmetry in the circulation of the lower atmosphere is most prominent.

The map sequence Fig. 2 should be compared with some previous evaluations of mixed layer depth in the tropical Atlantic. Robinson et al.'s (1979, charts 14, 26, 42, 56, 70, 84, 96, 112, 126, 140, 154, 168) calendar monthly maps have a one degree square spatial resolution, have different isopleth intervals, and extend southward only to 5°S. With these qualifications, major pattern characteristics are in good agreement with the present maps, Fig. 2. Lamb's (1984) maps are for bimonthly periods, possess a five degree square spatial resolution, and different isopleth intervals, and extend southward to 20°S. Within the limitations of the much coarser temporal and spatial resolution of his maps, they are found consistent with the maps of Fig. 2.

Recent modeling experiments and theoretical and empirical studies are directly relevant to the observed basinwide annual cycle of mixed layer depth documented in Fig. 2. Two major themes stand out: (i) variations in a vertical plane along the equator, and (ii) latitude shifts in thermal structure accompanying the seasonal migrations of the surface wind confluence over the equatorial North Atlantic. Merle (1980a,b) pointed
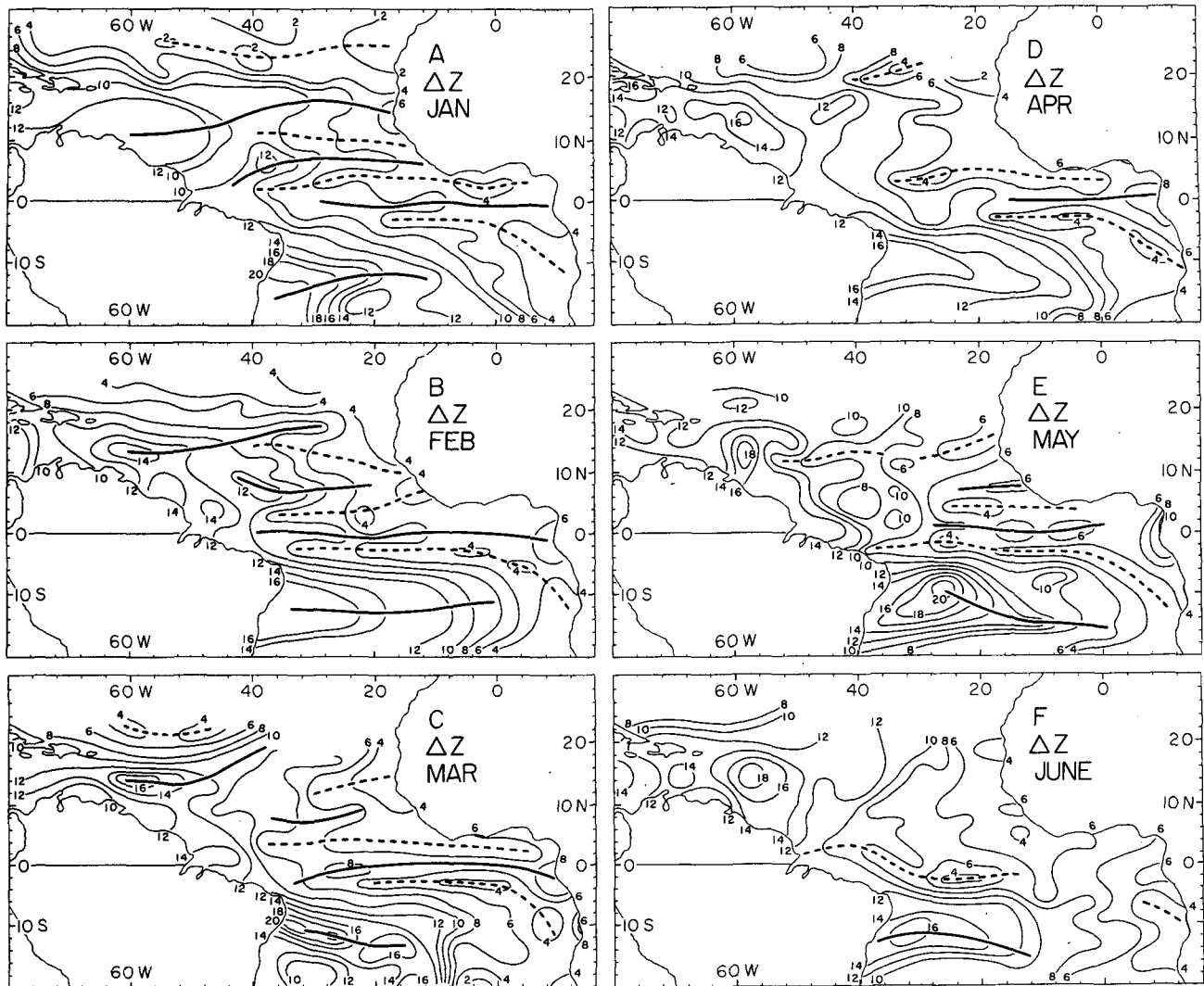
FIG. 4. Monthly maps of thermocline thickness in tens of meters. Heavy solid lines denote relative maxima, and heavy broken lines relative minima. Parts A–F: January, February, March, April, May, June.

out that variations of the easterly wind component along the equator are instrumental in depressing the isothermal surfaces from around the end of the boreal winter half-year towards the height of the summer, especially in the western portion of the basin. Concerning the low-latitude North Atlantic, where the poleward displacement of a zone of minimum mixed layer depth and the development of a ridge of maximum depth immediately to the north of the equator are particularly conspicuous from around April to August, Garzoli and Katz (1983), Philander and Pacanowski (1984) and du Penhoat and Tréguier (1984) demonstrated that the annual cycle of wind stress curl is responsible for changes in mixed layer depth and the seasonal reversal of the North Equatorial Countercurrent. Busalacchi and Picaut (1983) modeled the basinwide response of

the tropical Atlantic to the annual cycle of the surface wind field. Major seasonal characteristics reproduced include the zonal changes of pycnocline depth about a nodal point at the equator, and significant meridional contrasts in the timing of seasonal variations in the equatorial North Atlantic, all broadly consistent with Fig. 2. The comprehensive mapping of the annual cycle of mixed layer depth patterns thus has considerable relevance for recent and ongoing research on the tropical Atlantic.

b. Base of thermocline

Maps of thermocline base for all calendar months are shown in Fig. 3. Pattern characteristics differ considerably from those of mixed layer depth (Fig. 2), de-
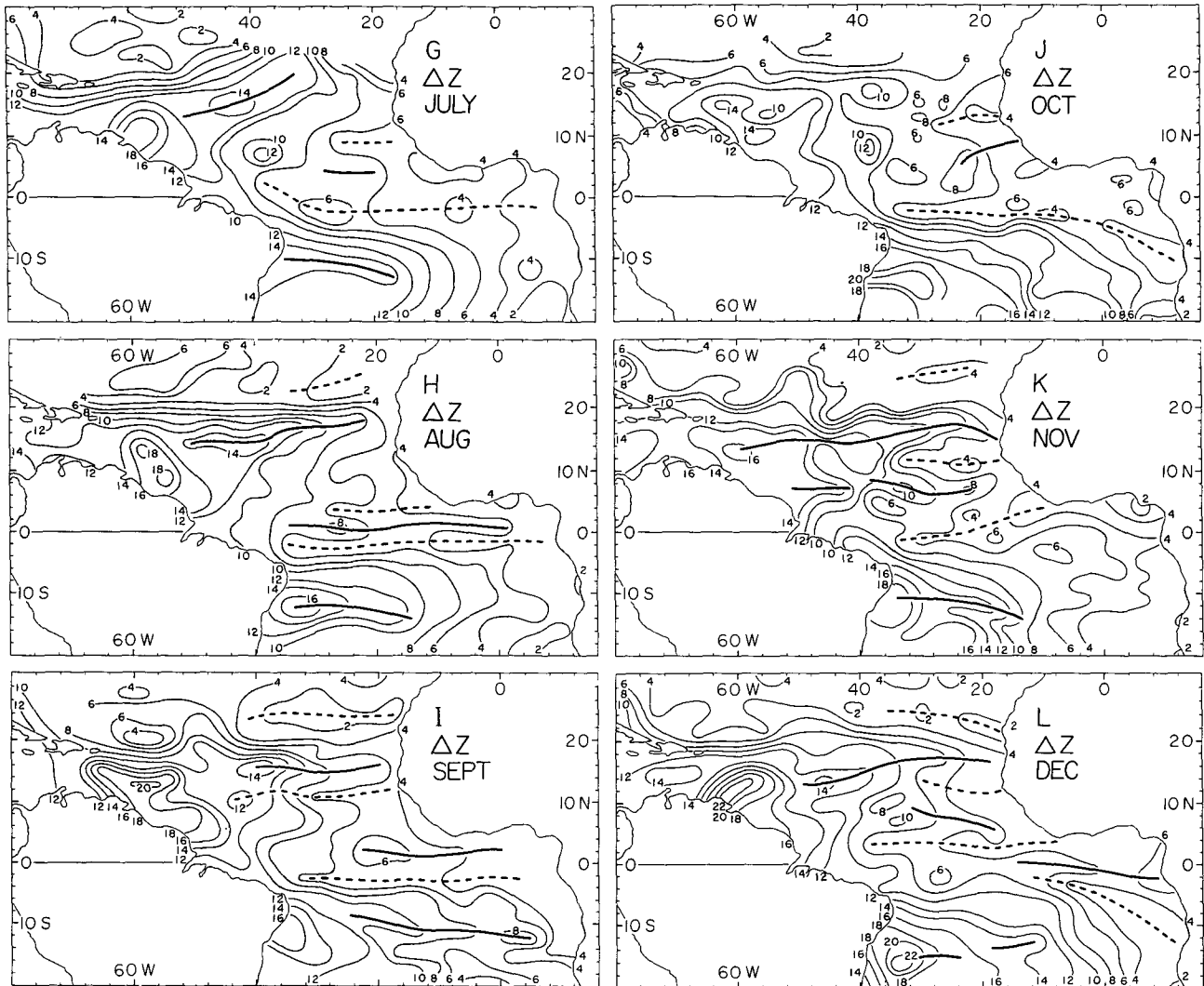
FIG. 4. (Continued). Parts G–L: July, August, September, October, November, December.

spite some similarities. As the mixed layer depth, the base of the thermocline tends to be deeper in the western as compared to the eastern portion of the basin, and overall it appears warped upward between about 15°N and 10°S. A band of smallest values extends from the coast of northern South America to West Africa. Particularly conspicuous is the evolution of a tongue of minimum values in the Eastern Atlantic immediately to the south of the equator from around February to September. This broadly underlies the cold water current extending from the coast of Southwest Africa into the equatorial Atlantic, and in July and August coincides with a similar feature in the patterns of mixed layer depth (Fig. 2) and sea surface temperature (Hastenrath and Lamb, 1977, charts 56–57). Within the overall upward warping of the thermocline base between about 15°N and 10°S, Fig. 3 then shows two zones of domings, one around 5°–10°N and the other at 0°–5°S.

The maps of thermocline base (Fig. 3) resemble the topography of the 20°C isothermal surface (not shown here), although pattern details are far from identical. The seasonal pattern changes of thermocline base (Fig. 3) appear also related to the annual march of subsurface heat storage Q_t in the layer surface to 500 m depth, as documented in Hastenrath and Merle (1986, maps Fig. 6). Some of the more prominent correspondences of patterns are as follows. From February to May, the thermocline base in the waters to the east of northern South America rises concomitant with a depletion of the oceanic heat content (Hastenrath and Merle, 1986, Fig. 6, parts B to E), while from May to September in this area the thermocline base deepens and the hydrospheric heat content increases. Broadly concurrently the thermocline base shallows in a zone poleward of about 10°N, where distinct heat depletion is indicated in July and August. Likewise, the rise of the thermocline base in the eastern equatorial Atlantic from May
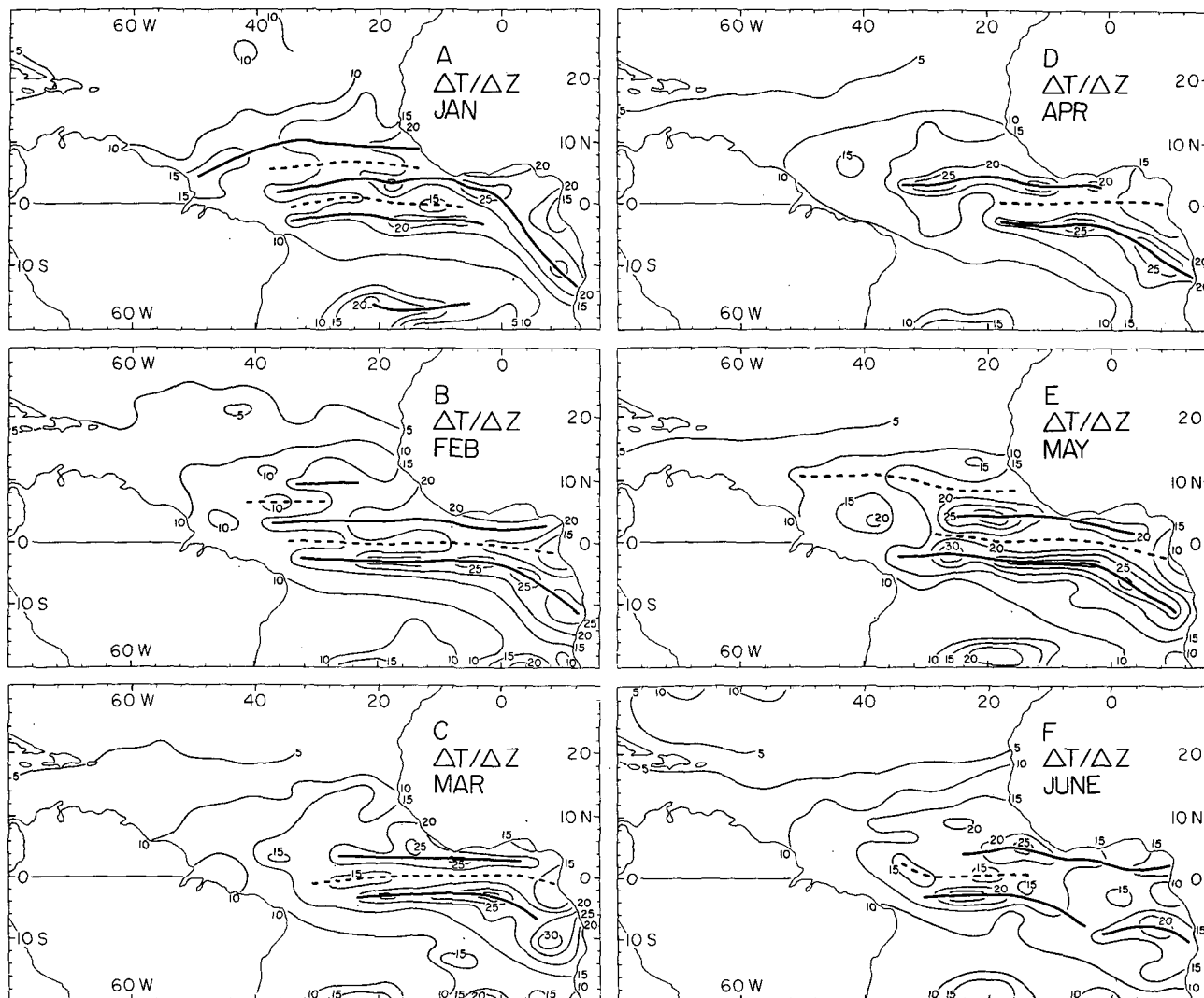
FIG. 5. Monthly maps of temperature gradient across the thermocline, in 10^{-2} °C m^{-1}. Heavy solid lines denote relative maxima, and heavy broken lines relative minima. Parts A–F: January, February, March, April, May, June.

to August is associated with a pronounced oceanic heat depletion in June and July. After September, a partly reversed evolution towards the February conditions takes place in the patterns of thermocline base and oceanic heat storage (Hastenrath and Merle, 1986, Fig. 6). The relation between the annual cycles of thermocline base and oceanic heat storage will be further considered in the discussion of vertical transects in sections 3e–g.

c. Thermocline thickness

The calendar monthly maps of thermocline thickness presented in Fig. 4 represent the difference between the thermocline base (Fig. 3) and the mixed layer depth (Fig. 2). There is an overall thinning of the thermocline from the western to the eastern side of the basin. During much of the year, broad bands of large thermocline

thickness are found around 15°N and 10°S. Equatorward from these broad, ill-defined zones of maximum values, distinct and narrow bands of thinnest thermocline stand out at about 4°N and S, separated by a ribbon of larger values along the Equator. The band of thinnest thermocline around 4°N is most prominent during the boreal winter half-year, while its Southern Hemisphere counterpart persists through most of the year. The narrow bands of thinnest thermocline (Fig, 4) are matched by maxima in the fields of vertical temperature gradient across the thermocline (section 3d; Fig. 5).

d. Temperature gradient across thermocline

The calendar monthly maps of the temperature gradient across the thermocline, Fig. 5, offer a measure of thermocline intensity. Throughout the year, the tem-
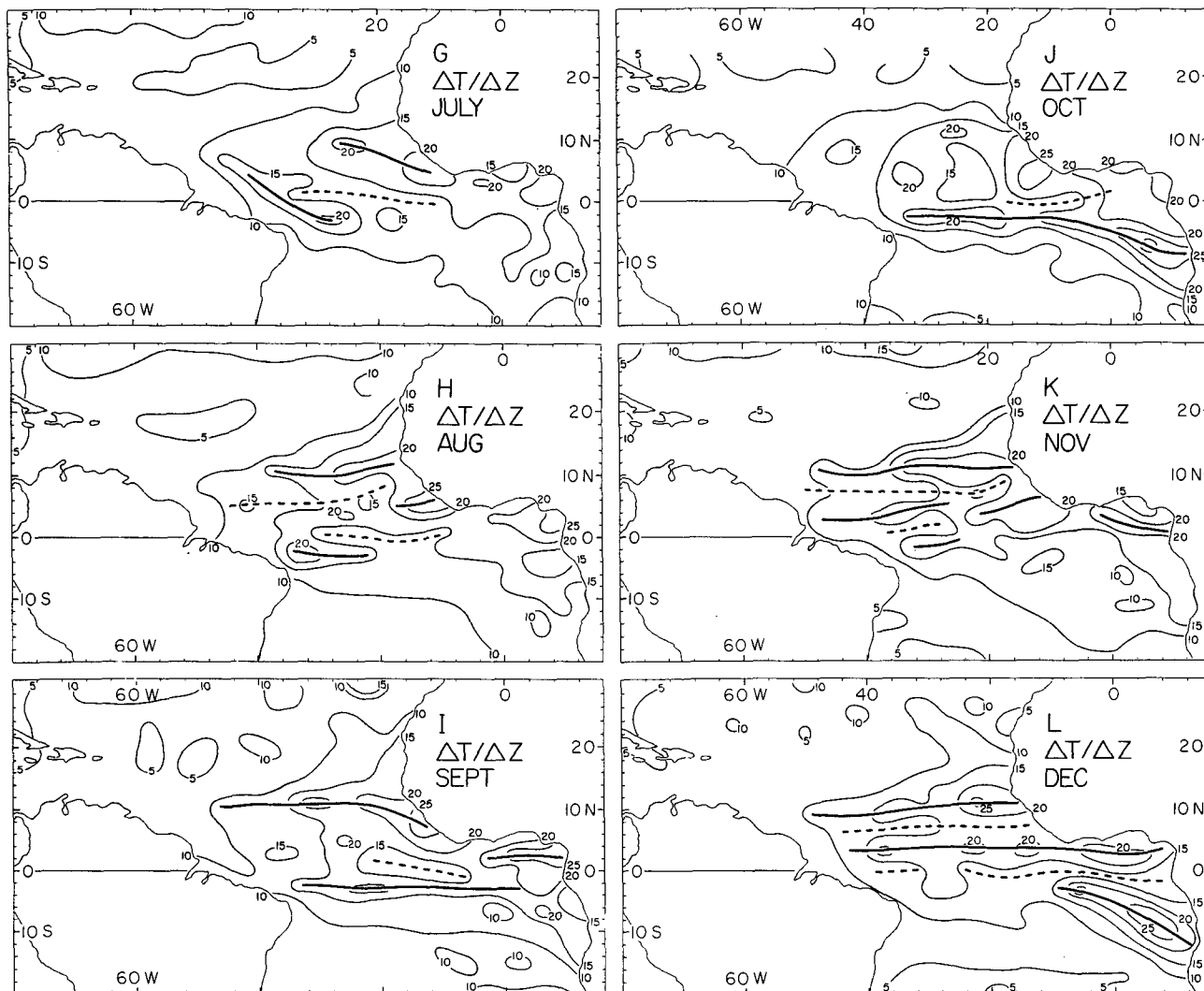
FIG. 5. (*Continued*). Parts G–L: July, August, September, October, November, December.

perature gradients are smallest at the northern and southern extremities of the map area, and comparatively large equatorward of 20°N and S. Comparison between Figs. 4 and 5 indicates that regions and months with a thin thermocline also tend to be characterized by comparatively steep vertical temperature gradients across the thermocline. Particularly striking in the map sequence of Fig. 5 are the extensive bands of most intense thermocline centered near 4°N and 4°S approximately symmetric to the equator, and separated by a narrow zone of much weaker thermocline along the equator. As the northern hemispheric band of thinnest thermocline (Fig. 4), the belt of maximum thermocline intensity around 4°N is best developed during the boreal winter semester (Fig. 5). Its southern hemispheric counterpart is prominent throughout much of the year except at the height of the boreal summer. As the southern hemispheric belt of thinnest thermocline, the

band of largest thermocline temperature gradient also bends, in its eastern portion, southeastward and extends to the coast of Southwest Africa.

e. Zonal cross sections along the Equator

The subsurface thermal structure in the equatorial zone of the Atlantic (Fig. 1, profile A) is documented in Fig. 6 by calendar monthly vertical cross sections along the equator, depicting selected isotherms along with the topographies of mixed layer depth and thermocline base as mapped in Figs. 2 and 3. Marked zonal contrasts persist throughout the year, as recognized in part previously by Merle (1980a,b, 1983), Katz (1981), and Houghton (1983). In the eastern portion of the transect, especially within the Gulf of Guinea, the mixed layer is shallow, and the thermocline thin and intense. By contrast, the western extremity of the cross
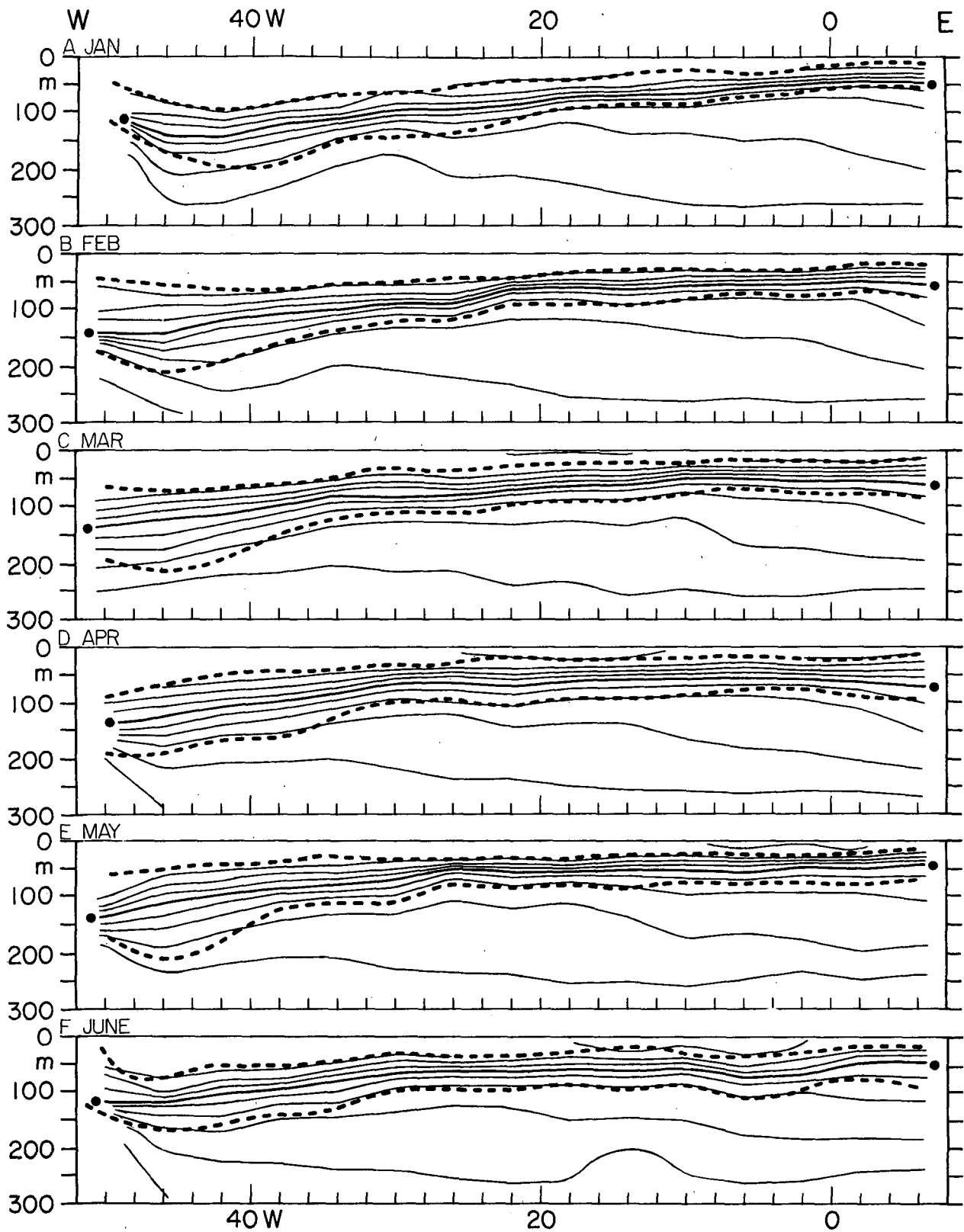
FIG. 6. Monthly zonal cross sections along the equator. See Fig. 1 for location of profiles (A-A). Thick solid lines with heavy dots at extremities represent 20°C isotherm, and thin solid lines other isotherms at 2°C intervals. Heavy broken lines denote the depth of the mixed layer and the base of the thermocline. Parts A-F: January, February, March, April, May, June.
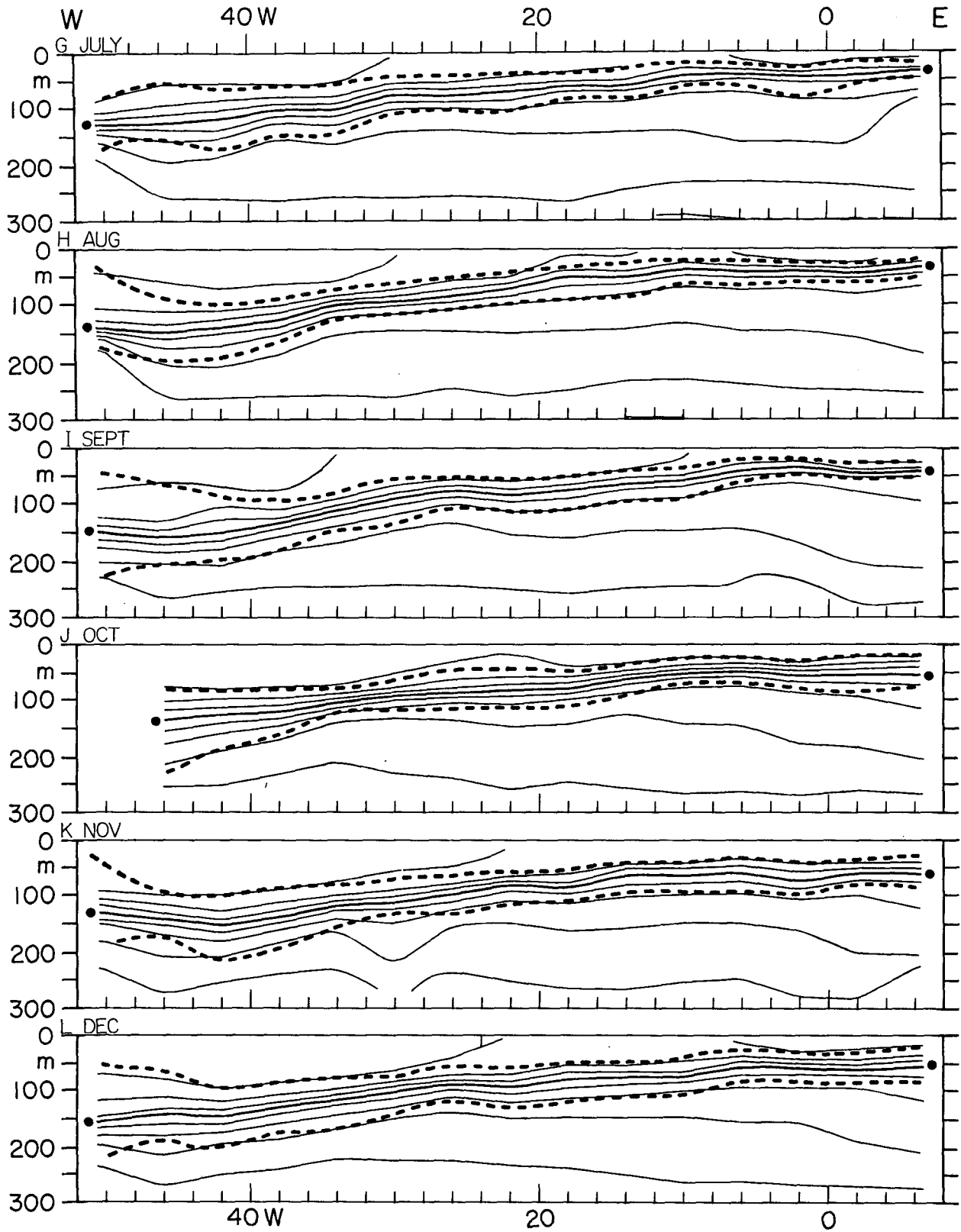
FIG. 6. (*Continued*). Parts G–L: July, August, September, October, November, December.

section, in particular the waters off the coast of Brazil, are characterized by a deep mixed layer, and a thick but comparatively weak thermocline.

From around April to August–September the thermocline thins, intensifies, and its base rises, especially in the eastern portion of the transect; to the west there is some tendency for a deepening of thermocline base and top. From after September to around April the thermocline thickens and weakens, its base deepens, again with particularly large effects in the eastern portion of the transect. The thermocline intensity in the west, and the mixed layer depth in all of the equatorial zone, vary comparatively little throughout the year. The implications of these annual cycle changes of subsurface thermal structure for the oceanic heat budget have been discussed by Merle (1980a,b) and Hastenrath and Merle (1986). In particular, the rise/drop of the thermocline base in the eastern/western portion of the transect from around April to August–September is associated with a depletion/storage of heat in the upper ocean (Hastenrath and Merle, 1986, Fig. 6, parts D–I), while from after September to around April (Fig. 6; Hastenrath and Merle, 1986, Fig. 6, parts I–L, A–D) the reverse evolution is indicated.

The calendar monthly vertical–zonal cross sections along the equator, Fig. 6, are complemented by the diagrams of the annual and longitudinal variation of subsurface structure, Fig. 7. This illustrates the overall deep mixed layer to the west, with greatest depth around the height of the boreal summer, and an overall shallow mixed layer to the east, with most extreme conditions also during the northern summer half year (Fig. 7, part a). The base of the thermocline (Fig. 7, part b) shows a pattern similar but not identical to that of mixed layer depth. The thermocline thickness (Fig. 7, part c) is overall largest in the west and least in the east, and these zonal contrasts become most pronounced during the boreal summer, when the thermocline stretches in the west and shrinks in the east.

f. Meridional cross sections across Eastern Atlantic

Calendar monthly meridional–vertical cross sections across the Eastern Atlantic (Fig. 1, profile B) are presented in Fig. 8. From around April to August–September, the thermocline immediately to the south of the equator thins, intensifies, and its base rises. After September, the thermocline in the equatorial region thickens and weakens, and its base deepens again.

The calendar monthly vertical–meridional cross sections across the Eastern Atlantic, Fig. 8, are complemented by the diagrams of the annual and latitudinal variation of subsurface thermal structure, Fig. 9. This shows the overall deepest mixed layer to the south and the much shallower depths in the equatorial region, as well as the shallowing from boreal winter to summer near the equator (Fig. 9a). The annual and latitudinal variation of the base of the thermocline (Fig. 9b) re-
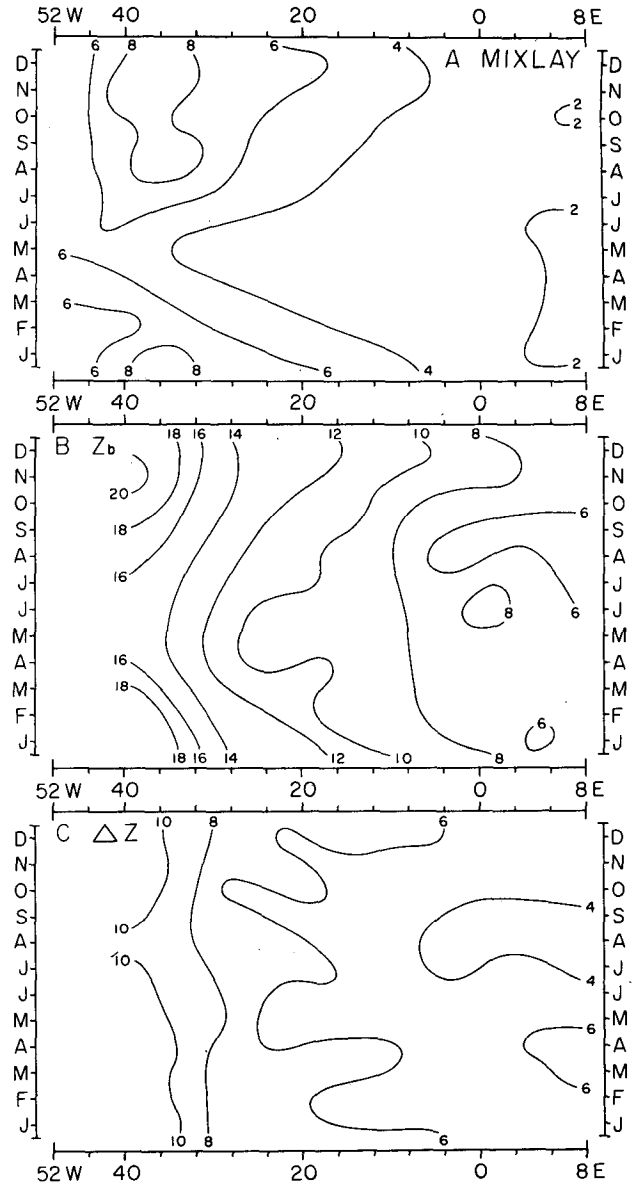

FIG. 7. Longitudinal and annual variation of subsurface thermal structure along profile A (ref. Fig. 1). Quantities are in tens of meters. (a) mixed layer depth MIXLAY; (b) base of thermocline z_b; (c) thermocline thickness Δz.

sembles that of the mixed layer depth (Fig. 9c). The thermocline thickness (Fig. 9c) is overall largest to the south and smaller in the equatorial region. A thin thermocline is encountered around 4°S throughout most of the year.

g. Meridional cross sections across the Central Atlantic

Meridional–vertical transects of the subsurface thermal structure in the central Atlantic (Fig. 1, profile C) are shown in Fig. 10. As indicated in Fig. 1, this profile (C) crosses the zonal-vertical profile (A) discussed in
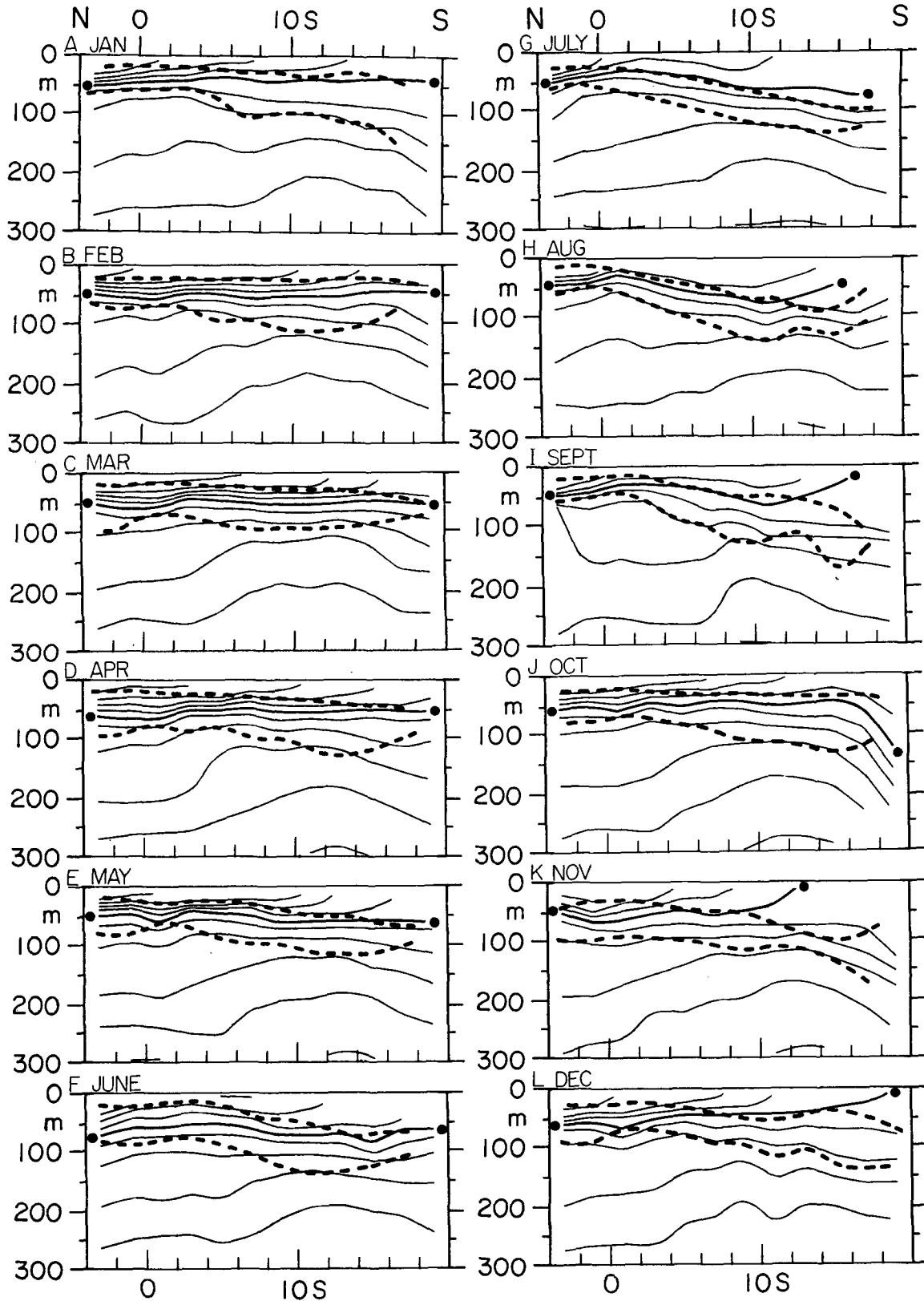
FIG. 8. Monthly meridional cross section across the eastern Atlantic. See Fig. 1 for location of profiles (B–B). Thick solid lines with heavy dots at extremities represent 20°C isotherm and thin solid lines other isotherms at 2°C intervals. Heavy broken lines denote the depth of the mixed layer and the base of the thermocline. Parts A–F: January, February, March, April, May, June; Parts G–L: July, August, September, October, November, December.
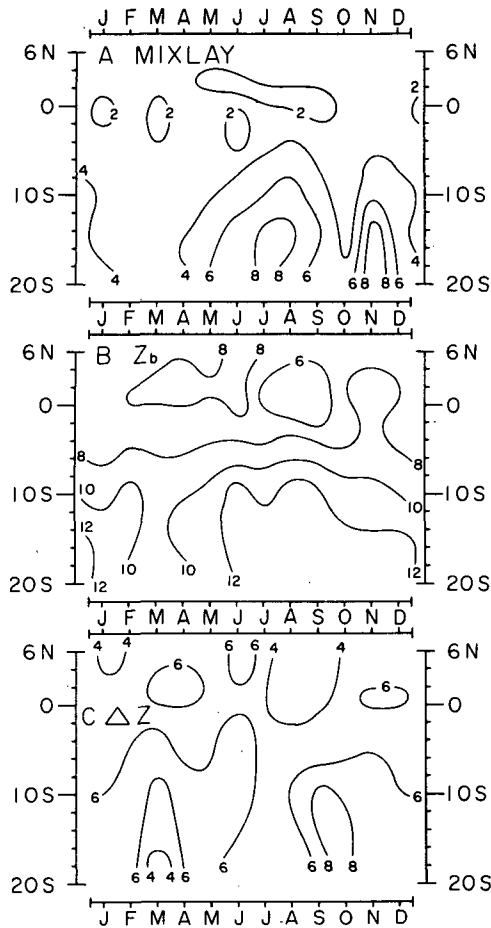
FIG. 9. Latitudinal and annual variation of subsurface thermal structure along profile B (ref. Fig. 1). Symbols as in Fig. 7.

section 3e (Fig. 6). The prominent year-round pattern characteristics are as follows. Mixed layer depth and thermocline base are shallowest in the equatorial North Atlantic, from where they deepen towards the northern and particularly the southern extremities of the profile. Overall, the thermocline is most intense in a zone immediately to the south of the equator and weakest at the northern and southern ends of the profile.

Around April, the domain of shallowest mixed layer and thermocline base and steepest vertical temperature gradient across the thermocline are found around 5°N. As one proceeds towards August–September, this domain gradually shifts to poleward of 10°N. Broadly concomitant with this is a shallowing of the thermocline base and a steepening of the vertical temperature gradient across the thermocline in a zone immediately to the south of the equator. After September, the domain of shallowest thermocline top and base and steepest vertical temperature gradient in the equatorial North Atlantic migrates southward, and in the zone immediately to the south of the equator the thermocline shallows and weakens.

The annual cycle of subsurface thermal structure documented in the meridional cross section (Fig. 10) appears related to the oceanic heat storage (Hastenrath and Merle, 1986, Fig. 6). As the domain of shallowest thermocline base migrates from around 5°N in April to poleward of 10°N in August so does a zone of oceanic heat depletion, or negative Q_t (Hastenrath and Merle, 1986, Fig. 6, parts D–H). After September, the reverse annual cycle development is indicated for both the thermocline base and the oceanic heat storage Q_t (Hastenrath and Merle, 1986, Fig. 6, parts I–L, A–D).

The calendar monthly vertical–meridional cross sections across the central Atlantic, Fig. 10, are complemented by the diagrams of the annual and latitudinal variation of subsurface thermal structure, Fig. 11. Overall, the mixed layer (Fig. 11a) is deepest in the southern portion and at the northern extremity of the profile and comparatively shallow in the equatorial region; in particular, the diagram illustrates the gradual northward displacement of the zone of shallowest mixed layer from around April to August–September. The annual variation of mixed layer depth along this profile across the central Atlantic depicted in Fig. 11, part a, resembles the annual cycle of heat storage averaged over latitude bands across the ocean (Hastenrath and Merle, 1986, Fig. 4, part b), in that meridional shifts of a zone of shallowest mixed layer are reflected in concomitant migrations of zones of heat depletion and storage. As in Figs. 7 and 9, the base of the thermocline (Fig. 11b) shows a pattern similar but not identical to that of the mixed layer depth (Fig. 11a). The thermocline thickness (Fig. 11c) exhibits an annual and latitudinal variation quite different from that of mixed layer depth (Fig. 11a). Overall the thermocline is thinnest in the equatorial region. Of particular interest are the extremely small values around 2–4°N and S, being most pronounced during the respective winter half-year. Figure 11 further illustrates that the extrema of thermocline thickness differ from those of mixed layer depth both by latitude and season.

4. Discussion and conclusions

This study used the most complete data bank presently available to ascertain spatial patterns and the annual cycle of subsurface thermal structure in the tropical Atlantic Ocean (30°N–20°S, east of 80°W). The basinwide patterns of temperature structure in the upper ocean were in the first place documented through the mapping of indicative parameters for all calendar months, namely mixed layer depth, base of thermocline, vertical distance from base to top of thermocline, and vertical temperature gradient across the thermocline. These maps were complemented by strategically placed vertical cross sections depicting base and top of thermocline and selected isotherms: a zonal transect along the equator extends from the African to the South
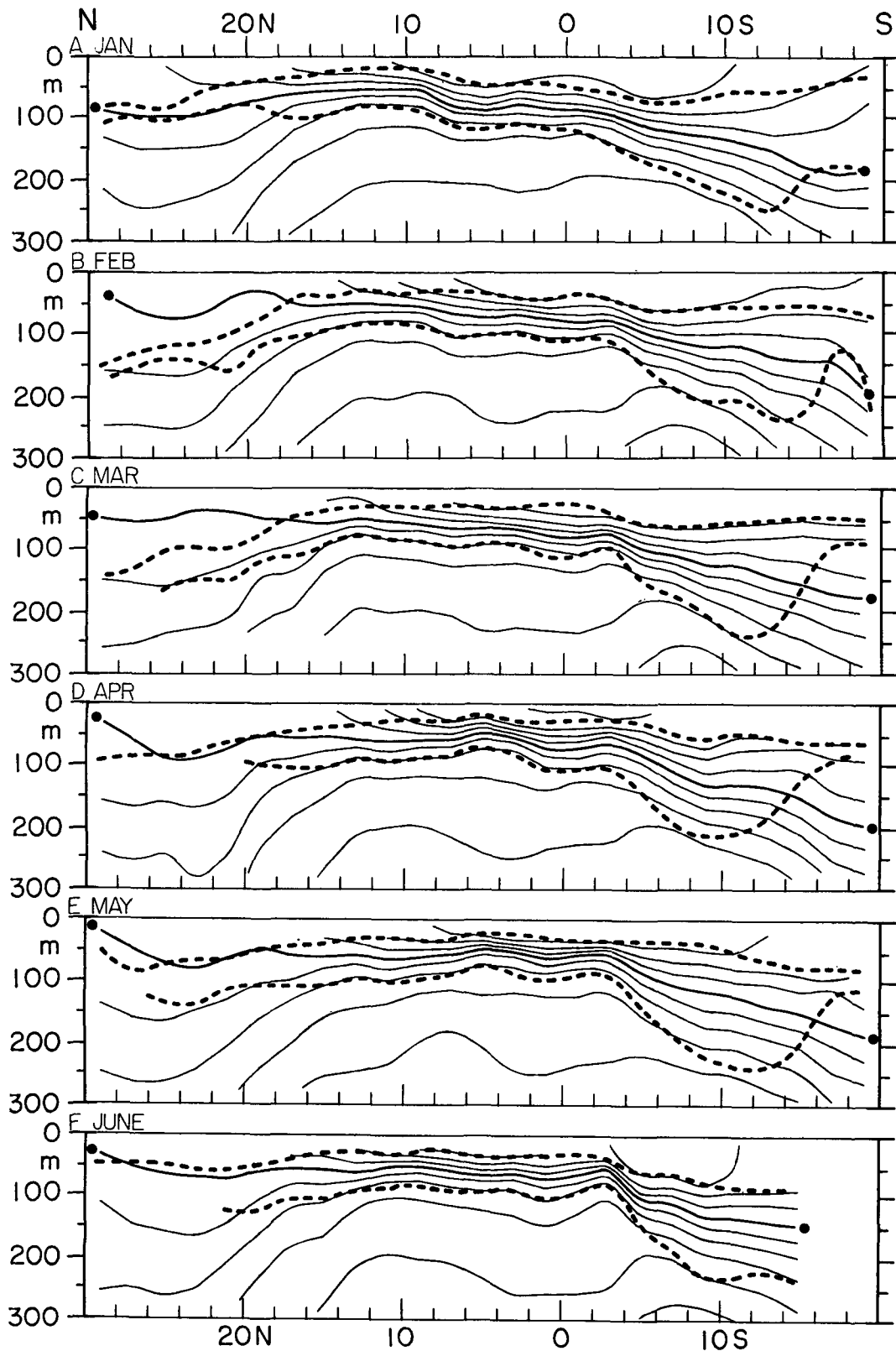
FIG. 10. Monthly meridional cross sections across the Central Atlantic. See Fig. 1 for location of profiles (C–C). Thick solid lines with heavy dots at extremities represent 20°C isotherm and thin solid lines other isotherms at 2°C. Heavy broken lines denote the depth of the mixed layer and the base of the thermocline. Parts A–F: January, February, March, April, May, June.
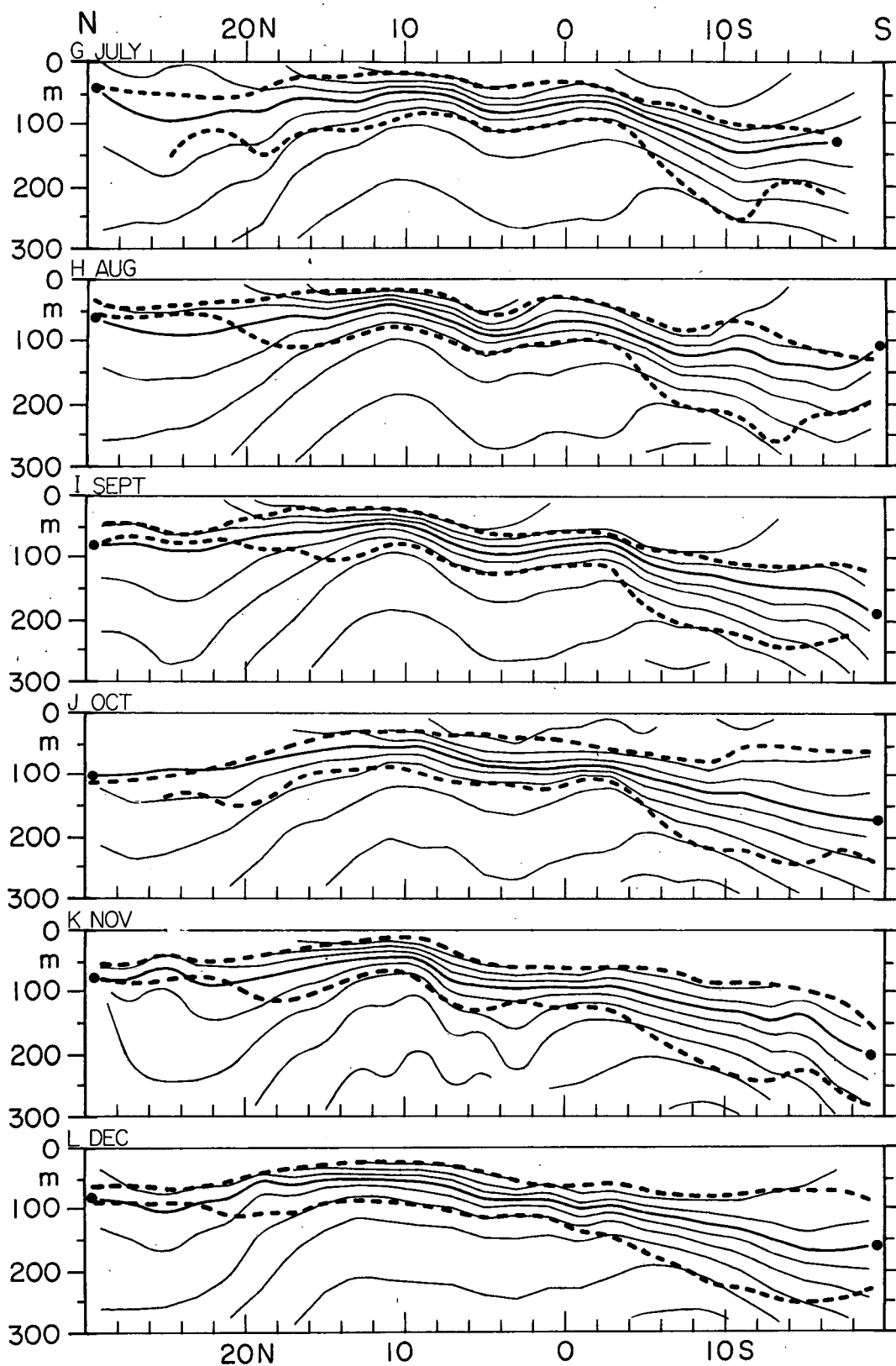
FIG. 10. (*Continued*). Parts G–L: July, August, September, October, November, December.
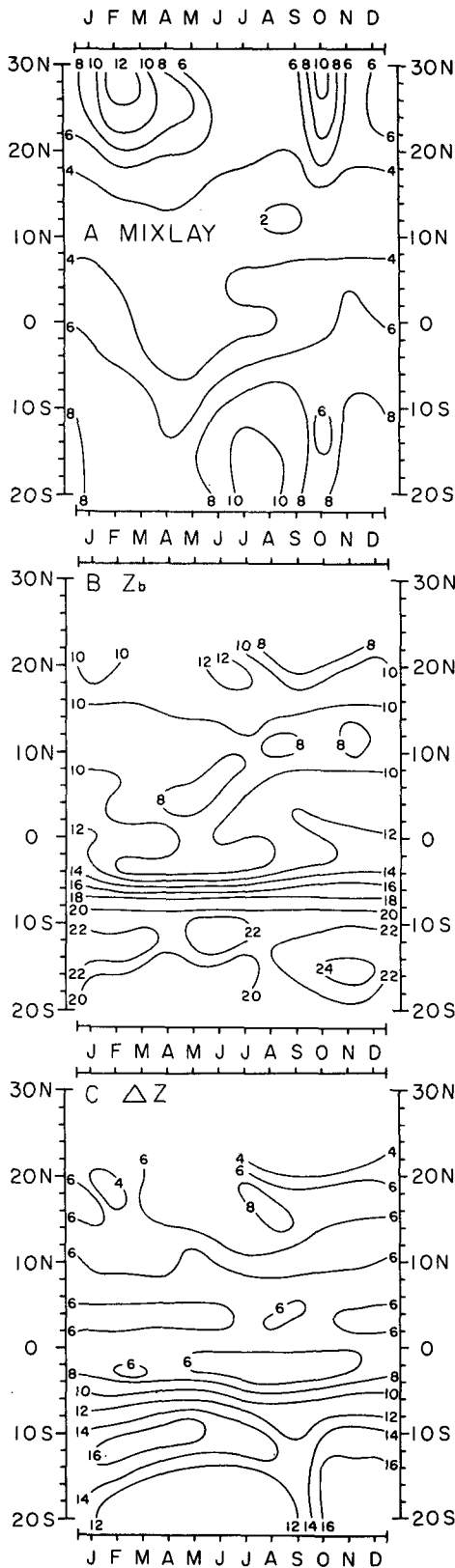
FIG. 11. Latitudinal and annual variation of subsurface thermal structure along profile C (ref. Fig. 1). Symbols as in Fig. 7.

American coast; a meridional profile centered on the Greenwich meridian stretches from the Gulf of Guinea southward; and a third, meridionally oriented section centered on 24°W cuts from the outer tropics of the Northern Hemisphere across the equatorial region into the South Atlantic.

Characteristic of the year as a whole is a relatively shallow mixed layer and thin and intense thermocline in the low latitudes, especially in the eastern part of the basin. The annual cycle of the surface wind field, with extrema around April and August, dominates the basinwide subsurface thermal structure in the tropical Atlantic. In the behavior of the mixed layer, the following systems of annual cycle variations stand out. In direct response to the annual variation of the zonal wind component in the equatorial zone the mixed layer depth along the Equator increases from around April to about August, with largest variations in the west. The northward migration of the wind confluence between the Northeast trades and the cross-equatorial airstreams from the Southern Hemisphere over the equatorial North Atlantic from April to August is accompanied by a northward migration of a zone of shallowest mixed layer and the development of a belt of maximum mixed layer depth immediately to the north of the equator. Advection of relatively warmer waters from the western portion of the basin appears instrumental in the buildup of this ridge of deep mixed layer. Furthermore, the evolution of this trough–ridge structure in mixed layer depth is related to the seasonal reversal of the North Equatorial Countercurrent. In the eastern Atlantic, seasonal variations are particularly pronounced in a zone immediately to the south of the equator. The annual cycle variations of mixed layer depth entail changes of oceanic heat content in the course of the year. Various numerical modeling experiments agree qualitatively with these observed annual cycle variations in the basinwide pattern of mixed layer depth.

The comprehensive documentation by maps and transects (Figs. 2–5, 8, 10), offered in sections 3a–d, f and g, bears out a remarkable structure of the thermocline near the equator. This diverse evidence is here placed in context and considered in relation to the motion field in the equatorial zone. A schematic synthesis of thermal structure and zonal and vertical motion is presented in Fig. 12.

The top of the thermocline, while standing highest well to the north of the equator year round, is warped upward at the equator and downward around 4°N, especially around January–February and July–September. The base of the thermocline exhibits a doming at about 4°S throughout much of the year, distinctly greater depth at the equator, and another doming in the Northern Hemisphere, being near 4°N around the end of the boreal winter semester, but as far poleward as 10°N at the height of the boreal summer. Implicit in these patterns of thermocline top and base are

marked meridional variations in thermocline thickness and intensity (Figs. 2-5, 10). Thus, a zone of relatively thick and weak thermocline is found along the Equator, and a band of thin thermocline and isotherm packing at 4°S, throughout much of the year (Figs. 4, 5, 10), while a zone of thin and intense thermocline around 4°N appears most prominently during the boreal winter semester (Figs. 4, 5, 10). These peculiarities in near-equatorial thermocline structure are not explained or in fact recognized in the numerical studies referred to in section 3b.

Figure 12 further sketches the characteristic equatorward plunging of isotherms and associated column of weak vertical temperature gradient below the thermocline and within a few degrees from the equator known as "thermostad," and apparent in the meridional–vertical cross sections (Fig. 10). Consistent with the implied mass distribution, eastward flowing subsurface countercurrents (SSCC) are centered on the poleward flanks and the upper edge of the thermostad, at a typical depth of around 170 m and latitudes of

4°N and 4°S (Hisard et al., 1976; Cochrane et al., 1979; Molinari, 1982; Hisard and Hénin, 1984). Further entered in Fig. 12 is the core of the likewise eastward flowing Equatorial Undercurrent (EUC) within the thermocline, which is understood as being due to westward wind stress and resulting eastward pressure gradient within the thermocline along the equator.

An issue which begs explanation is the origin of the narrow zones of thin and intense thermocline around 4°N and 4°S, contrasting with the much thicker and weaker thermocline near the equator. This problem is discussed here with reference to the synthesized meridional–vertical cross section Fig. 12. A satisfactory understanding of causalities is as yet lacking; in fact, the present empirical findings invite a thorough theoretical investigation. However, McPhaden's (1984) modeling study may enlighten the pertinent processes.

McPhaden (1984) forced a linear steady-state equatorial (1–3 deg latitude) model by hemispherically symmetric curl-free easterly winds, and succeeded in reproducing much of the observed subsurface zonal
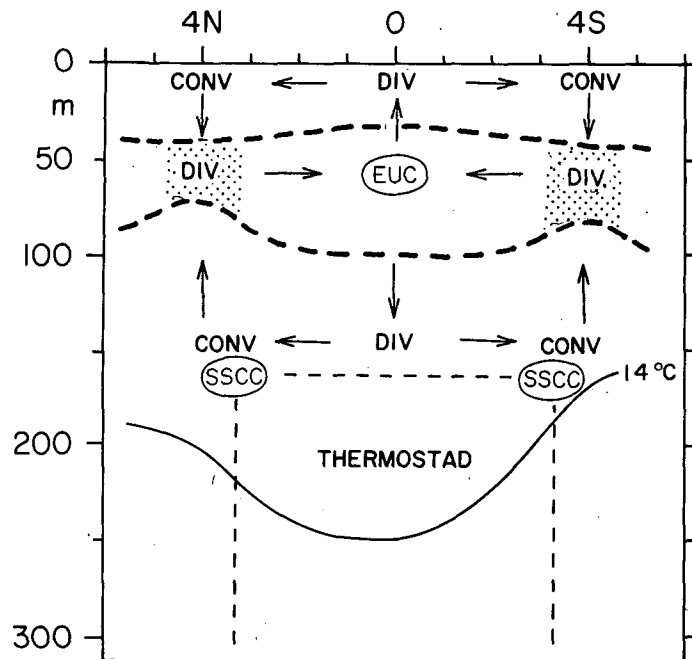

FIG. 12. Schematic meridional–vertical cross section of subsurface temperature and flow structure, synthesized from the present analysis of subsurface temperature soundings, observations of zonal currents (Hisard et al., 1976; Cochrane et al., 1979; Molinari, 1982; Hisard and Hénin, 1984), and numerical modelling (McPhaden, 1984). Heavy broken lines denote base of mixed layer and base of thermocline, dot raster regions of maximum vertical temperature gradient, thin solid line 14°C isotherm, and thin broken line the thermostad, all from the present analysis of subsurface temperature soundings. Ellipses indicate the cores of the eastward directed Equatorial Undercurrent EUC and of the Subsurface Countercurrents SSCC (sources: Hisard et al., 1976; Cochrane et al., 1979; Molinari, 1982; Hisard and Hénin, 1984). Horizontal divergence and convergence is indicated by DIV and CONV, respectively, and meridional and inferred vertical flow components by arrows (source: McPhaden, 1984).

current structure. He also produced model meridional velocities, which are schematically entered in Fig. 12. At the surface, Ekman divergence commensurate with the surface easterlies prevails up to about 1.5 deg latitude. At the level of the EUC, there is geostrophic convergence within about 1.5 degrees from the equator, driven by the zonal pressure gradient off the equator, giving way to divergence beyond these latitudes. In the depth range of the SSCC, there is a poleward geostrophic flow in both hemispheres consistent with the downward reversal of the pressure gradient. At these depths divergence is found within about 1 to 1.5 deg latitude from the equator, giving way to convergence further poleward. Also sketched in Fig. 12 is the vertical motion pattern inferred from the horizontal divergence and convergence distribution obtained in McPhaden's (1984) model experiment. This seems directly related to the characteristic near-equatorial thermocline structure synthesized in Fig. 12. Near the equator, vertical motion is upward above, but downward below the EUC. Beyond about 1.5 deg latitude there is marked horizontal divergence at the level of the EUC, or in the thermocline layer and this appears compensated by upwelling from the depths of the SSCC and downwelling in the shallow surface layer in which the marked near-equatorial divergence gives way to weak convergence beyond about 1.5 deg latitude.

A sketch of possible causal relationships in the peculiar near-equatorial thermocline structure is proposed in the following by way of working hypothesis. Surface easterly winds cause Ekman divergence and upwelling at the equator, as well as a pile-up of waters and a rise of isobaric surfaces toward the west. Due to the poleward increase of the Coriolis parameter, the meridional surface Ekman transport changes to convergence and downwelling at a few degrees from the equator. Such a vertical motion field in the mixed layer is conducive to the observed upward bulging of the thermocline top at the equator and the downward warping around 4°N and 4°S. The zonal pressure gradient causes the eastward flowing EUC at the equator and also an equatorward geostrophic flow at the level of the EUC with divergence some distance away from and convergence at the equator. The convergence within the thermocline at the equator is compensated by the aforementioned equatorial upwelling in the mixed layer, and downwelling from the thermocline downward. This gives way to upwelling at some distance away from the equator, below the thermocline. Such a vertical motion pattern is conducive to the observed equatorward plunging of isotherms a few degrees away from the Equator and the origin of the column of relatively warm and weakly stratified waters of the thermostad. The implicit mass and pressure distribution is commensurate with eastward geostrophic currents centered at the poleward and upper edges of the thermostad. Directly relevant to the observed near-equatorial thermocline structure as synthesized in Fig.

12 is the realization that easterly surface winds are capable of producing at the Equator upwelling above and downwelling below the thermocline, a vertical spreading of isotherms, and thus a thick and weak thermocline, while leading to contrastingly different vertical motion and thermal conditions a few degrees away from the Equator. These are characterized by downwelling above and upwelling below the thermocline and hence a packing of isothermal surfaces, upward warping of the thermocline base and downward bulging of thermocline top, and thus a thin and intense thermocline.

It is noted from the empirical documentation, Figs. 4, 5, 10, that the simple, hemispherically symmetric pattern synthesized in Fig. 12 is not obtained throughout the year. While the southern hemispheric extremum of thermocline thickness and intensity prevails year round, its northern hemispheric counterpart is best developed in the latter part of the boreal winter semester but absent at the height of the boreal summer. In this context it is recalled that the surface wind field is least asymmetric with respect to the equator around the end of the boreal winter half-year, whereas at the height of the summer the confluence between the northeast trades and the cross-equatorial airstreams from the Southern Hemisphere is displaced far poleward and a pronounced pattern of wind stress curl dominates over the equatorial North Atlantic (Hastenrath and Lamb, 1977, charts 42–49). It is here conjectured that the seasonally varying hemispheric asymmetry of the surface wind field is a major factor for the appearance and vanishing, in the course of the year, of the northern hemispheric extremum of thermocline thickness and intensity. These and related problems invite more extensive theoretical investigations. It is expected that the present comprehensive documentation of the observed annual cycle of subsurface thermal structure may provide a useful reference for further empirical and modeling studies of the upper hydrosphere in the tropical Atlantic.

REFERENCES

Anonymous, 1981: *Seasonal equatorial Atlantic experiment.* Lamont-Doherty Geological Observatory, Palisades, N.Y., 39 pp.
——, 1984: Plan for the TOGA scientific programme, working draft. (Intergovernmental Oceanographic Commission, World Meteorological Organization, Committee on Ocean Research, International Council of Scientific Unions), JSC/CCCO TOGA Scientific Steering Group, Paris, 150 pp.

Busalacchi, A. J., and J. Picaut, 1983: Seasonal variability from a model of the tropical Atlantic ocean. *J. Phys. Oceanogr.* **13**, 1564–1588.

Cane, M. A., and R. J. Patton, 1984: A numerical model for low-frequency equatorial dynamics. *J. Phys. Oceanogr.* **14**, 1853–1863.

Cochrane, J. D., F. J. Kelly and C. R. Olling, 1979: Subthermocline countercurrents in the western equatorial Atlantic Ocean. *J. Phys. Oceanogr.*, **12**, 1388–1410.

du Penhoat, Y., and A. M. Tréguier, 1984: Sea surface dynamic height topography and the North Equatorial Countercurrent as inferred from a linear model. *Geophys. Res. Lett.*, **11**, 799–801.

Garzoli, S. L., and E. J. Katz, 1983: The forced annual reversal of the Atlantic North Equatorial Countercurrent. *J. Phys. Oceanogr.*, **13**, 2082–2090.

Hastenrath, S., 1984: Interannual variability and annual cycle: mechanisms of circulation and climate in the tropical Atlantic sector. *Mon. Wea. Rev.*, **112**, 1097–1107.

——, and P. J. Lamb, 1977: *Climatic Atlas of the Tropical Atlantic and Eastern Pacific Oceans*. University of Wisconsin Press, 112 pp.

——, and ——, 1978: *Heat Budget Atlas of the Tropical Atlantic and Eastern Pacific Oceans*. University of Wisconsin Press, 104 pp.

——, and J. Merle, 1986: On the annual march of heat storage and export in the tropical Atlantic Ocean. *J. Phys. Oceanogr.*, **16**, 694–708.

Hisard, P., and C. Hénin, 1984: Data set of the first FOCAL cruises. July 1982–November 1983. ORSTOM, 86 pp.

——, J. Citeau and A. Morlière, 1976: Le système de contre-courants équatoriaux subsuperficiels; permanence et extension de la branche sud dans l'Océan Atlantique. *Cah. ORSTOM, sér. Oceanogr.*, vol. 14, no. 3, 209–220.

Houghton, R. W., 1983: Seasonal variation of the subsurface thermal structure in the Gulf of Guinea. *J. Phys. Oceanogr.*, **13**, 2070–2081.

Katz, E. J., 1981: Dynamic topography of the sea surface in the equatorial Atlantic. *J. Mar. Res.*, **39**, 53–63.

Lamb, P., 1984: On the mixed layer climatology of the North and tropical Atlantic. *Tellus*, **36A**, 292–305.

——, and A. F. Bunker, 1982: The annual march of the heat budget of the North and tropical Atlantic Oceans. *J. Phys. Oceanogr.*, **12**, 1388–1410.

Levitus, S., 1982: *Climatological Atlas of the World Ocean*. NOAA Prof. Paper No. 13, Rockville, Md., 173 pp.

——, 1984: Annual cycle of temperature and heat storage in the World ocean. *J. Phys. Oceanogr.*, **14**, 727–746.

McPhaden, M. J., 1984: On the dynamics of equatorial subsurface countercurrents. *J. Phys. Oceanogr.*, **14**, 1216–1225.

Merle, J., 1980a: Seasonal heat budget in the equatorial Atlantic Ocean. *J. Phys. Oceanogr.*, **10**, 464–469.

——, 1980b: Seasonal variation of heat storage in the tropical Atlantic Ocean. *Oceanol. Acta*, **3**, 455–463.

——, 1980c: Programme Français Océan Atlantique Équatorial. mimeographed.

——, 1983: Seasonal variability of subsurface thermal structure in the tropical Atlantic Ocean. *Proc. of the 14th Annual Liège Colloq. on Ocean Hydrodynamics*, J. C. G. Nihoul, Ed., Elsevier, 31–50.

——, and S. Arnault, 1985: Seasonal variability of the surface dynamic topography in the tropical Atlantic Ocean. *J. Mar. Res.*, **43**, 267–288.

Molinari, R. L., 1982: Observations of eastward currents in the tropical South Atlantic Ocean: 1978–80. *J. Geophys. Res.*, **87**(C12), 9701–9714.

Moore, D., P. Hisard, J. McCreary, J. Merle, J. O'Brien, J. Picaut, J. M. Verstraete and C. Wunsch, 1978: Equatorial adjustment in the eastern Atlantic. *Geophys. Res. Lett.*, **5**, 637–640.

National Academy of Sciences, National Research Council, 1983: El Niño and Southern Oscillation; a scientific plan. National Academy Press, Washington, DC, 72 pp.

National Climate Program Office, NOAA, 1980: *National Climate program, five-year plan*. Washington, DC, 101 pp.

Philander, G., 1978: Upwelling in the Gulf of Guinea. *J. Mar. Res.*, **37**, 23–33.

Philander, S. G. H., and R. C. Pacanowski, 1984: Simulation of the seasonal cycle in the tropical Atlantic Ocean. *Geophys. Res. Lett.*, **11**, 802–804.

Robinson, M., R. Bauer and E. Schroeder, 1979: *Atlas of North Atlantic-Indian Ocean monthly mean temperatures and mean salinities of the surface layer*. Naval Oceanographic Office, NOO RP-18, NSTL Station, Bay St. Louis, Missouri, 39422, 234 pp.

Servain, J., J. Picaut and J. Merle, 1982: Evidence of remote forcing in the equatorial Atlantic Ocean. *J. Phys. Oceanogr.*, **12**, 457–463.

Weisberg, R. H., and T. Y. Tang, 1983: Equatorial ocean response to growing and moving wind systems with application to the Atlantic. *J. Mar. Res.*, **41**, 461–486.

World Meteorological Organization, 1980: *Outline plan and basis for the World Climate Programme*, 1980–83. Geneva, WMO—No. 540, 64 pp.

World Meteorological Organization—ICSU, 1983: Large-scale oceanographic experiments in the WCRP. WCRP Publ. Ser. No. 1, 2 vols., (vol. 1, p. 1–20).

Wyrtki, K., 1971: *Oceanographic Atlas of the International Indian Ocean Expedition*. National Science Foundation, Washington, DC, 531 pp.